Materials Today Bio 2 (2019) 100006

Contents lists available at ScienceDirect

Materials Today Bio

journal homepage: www.journals.elsevier.com/materials-today-bio

Engineering human stellate cells for beta cell replacement therapy promotes *in vivo* recruitment of regulatory T cells

D.C. Oran [a], T. Lokumcu [a], Y. Inceoglu [d], M.B. Akolpoglu [d], O. Albayrak [b], T. Bal [a], M. Kurtoglu [c,f], M. Erkan [c,e], F. Can [b,c,e], T. Bagci-Onder [a,c,e], S. Kizilel [a,d,e,*]

[a] Biomedical Science and Engineering, Koc University, Sariyer 34450, Istanbul, Turkey
[b] Medical Microbiology, School of Medicine, Koc University, Sariyer 34450, Istanbul, Turkey
[c] Koc University, School of Medicine, Department of Surgery, Zeytinburnu 34010, Istanbul, Turkey
[d] Chemical and Biological Engineering, Koc University, Sariyer 34450, Istanbul, Turkey
[e] Koc University, Research Center for Translational Medicine (KUTTAM), Sariyer 34450, Istanbul, Turkey

ARTICLE INFO

Keywords:
Islet transplantation
Immune engineering
Regulatory T cells
Stellate cells
CCL22

ABSTRACT

Type 1 diabetes (T1D) is an autoimmune disease characterized by destruction of pancreatic β cells. One of the promising therapeutic approaches in T1D is the transplantation of islets; however, it has serious limitations. To address these limitations, immunotherapeutic strategies have focused on restoring immunologic tolerance, preventing transplanted cell destruction by patients' own immune system. Macrophage-derived chemokines such as chemokine-ligand-22 (CCL22) can be utilized for regulatory T cell (Treg) recruitment and graft tolerance. Stellate cells (SCs) have various immunomodulatory functions: recruitment of Tregs and induction of T-cell apoptosis. Here, we designed a unique immune-privileged microenvironment around implantable islets through overexpression of CCL22 proteins by SCs. We prepared pseudoislets with insulin-secreting mouse insulinoma-6 (MIN6) cells and human SCs as a model to mimic naive islet morphology. Our results demonstrated that transduced SCs can secrete CCL22 and recruit Tregs toward the implantation site *in vivo*. This study is promising to provide a fundamental understanding of SC-islet interaction and ligand synthesis and transport from SCs at the graft site for ensuring local immune tolerance. Our results also establish a new paradigm for creating tolerable grafts for other chronic diseases such as diabetes, anemia, and central nervous system (CNS) diseases, and advance the science of graft tolerance.

Introduction

Type 1 diabetes (T1D) is an autoimmune disease caused by destruction of insulin-secreting islets in the pancreas, resulting in insulin deficiency and high blood glucose [1–4]. The immune system of patients with T1D recognizes islets as foreign substances, which is caused by the release of β-cell antigens due to stress, viral infection, or proinflammatory cytokines released from islet cells. Those antigens are presented by antigen-presenting cells (APCs), and these APCs activate $CD8^+$ T cells. Activated $CD8^+$ T cells migrate toward pancreatic islets where they recruit and activate lymphocytes and macrophages and induce proapoptotic signaling and death of β-cells [5,6].

Alternative to whole-pancreas transplantation, isolation and transplantation of insulin-secreting islets from cadaveric human donors is promising to treat T1D; however, the need for systemic suppression of the immune system of the recipient patients and limited availability of donor islet tissue are the main challenges in clinics [7]. To overcome immunosuppression requirement and to prevent destruction of transplanted β cells, immunotherapeutic strategies have considered immunologic tolerance approaches [1,2,8–11]. Regulatory T cells (Tregs) are the main actors in the tolerance of implanted tissue because they have significant functions in the suppression of autoreactive immune responses and maintenance of self-tolerance [6,12]. For example, in a previous study, $CD4^+CD25^+FoxP3^+$ T cells alleviated the progress of T1D through diminished autoimmune attack and provided graft tolerance [13,14]. In another study, the loss of function and decrease in the number of Tregs were observed in pancreatic lymph nodes rather than in peripheral blood of diabetic patients, which suggested the role of Tregs in autoimmune

* Corresponding author. Biomedical Science and Engineering, Koc University, Sariyer 34450, Istanbul, Turkey.Fax: +90 212 338 1548.
E-mail address: skizilel@ku.edu.tr (S. Kizilel).
[f] Current address: Cartesian Therapeutics Inc. MD, USA

https://doi.org/10.1016/j.mtbio.2019.100006
Received 28 January 2019; Received in revised form 2 May 2019; Accepted 2 May 2019
Available online 23 May 2019

diseases [6]. In our previous studies, we developed a technique to coat islets with Tregs without hindering viability and functionality for local immunoprotection of islets [15,16]. Tregs are important for maintenance of immunity and self-tolerance; however, optimal suppressive function of Tregs *in vivo* requires trafficking and migration to tissues and secondary lymphoid organs [17,18]. One of the concerns about cotransplantation of islets with Tregs involves proliferation of Tregs from the recipient patient. Technically, isolation and proliferation of Tregs is possible; however, isolation of islets from a deceased donor could not be planned ahead. Recent efforts from Treg cryopreservation studies proved that repeated freezing and thawing of Tregs might have negative influences on the expression of the two receptors (L-selectin [CD62L] and CCR5), cytokine production, and interleukin (IL)-2 secretion which are all critical for the suppressive function of Tregs [19,20]. Considering the drawbacks of Treg cryopreservation, infusion of Tregs with islets during pancreatic islet transplantation does not appear to be a feasible option.

Recently, it has been demonstrated that similar immunosuppressive mechanisms operate in cancer microenvironment. Cancer cells adopt a reverse strategy, and they escape immune destruction by modulating their local environment and developing tolerance through secretion of chemokines. For example, cancer cells express CCL22, a macrophage-derived chemokine (MDC), and mediate recruitment of Tregs to the tumor site [21–23].

To address limited supply of insulin-secreting islets, alternative pancreatic β cell lines have been considered in previous studies. For example, murine cell lines such as MIN6 cells have been frequently used for development of insulin-secreting graft models [4]. Accessory cells such as mesenchymal stem cells and stellate cells (SCs) have also been explored to provide graft tolerance in islet transplantation [24–26]. For example, hepatic SCs (HSCs) have immunomodulatory activity, and they can promote expansion of Tregs, suppression of T cells, and induction of T-cell apoptosis. SCs can also promote angiogenesis, secreting proangiogenic factors such as vascular endothelial growth factor (VEGF) [27–29]. It has been shown that cotransplantation of HSCs can prevent islet allograft rejection via formation of an immune barrier [30–34]. However, only few studies investigated the effects of pancreatic SCs (PSCs) on pancreatic β cells, although these cells have also been reported to contribute to immune evasion in pancreatic cancer indirectly. They have been shown to sequester $CD8^+$ T cells in pancreatic cancer stroma, recruit myeloid-derived suppressor cells into stroma, and induce apoptosis of T cells [35–37]. Kikuta et al. [38] have shown that coculture of PSCs with RIN5F rat pancreatic β cells impairs their function by reducing insulin expression and promoting apoptosis. Zang et al. [39] have reported similar effects of PSCs on insulin secretion function of mouse islets.

In this study, we developed a new approach to provide local immunomodulation for islet grafts through recruitment of Tregs by secretion of the chemokine CCL22 from SCs. Intrinsic immunomodulatory characteristics of SCs were combined with the secretion of CCL22 protein to obtain an immunologically privileged microenvironment. We considered this approach as a better one than simultaneous transplantation of islets and Tregs **(**Fig. 1A**)**. We addressed challenges associated with repeated islet isolation through preparation of heterospheroids with MIN6 cells. MIN6 cells have been reported as a valid model that can mimic naive islet morphology and function [40,41]. To achieve Treg recruitment, human PSCs (hPSCs) and human HSCs (hHSCs) were transduced to express CCL22 before *in vivo* experiments and then pseudoislets were prepared with MIN6 cells and transduced SCs by the hanging drop method (Fig. 1B). The study presented here represents a major leap forward from the existing approaches by introducing a novel dynamic islet-SC system based on the synthesis and release of bioactive proteins within an islet microenvironment. This strategy enables interaction of multiple cell types to create an adaptive biointerface where insulin secretion and graft tolerance can be achieved simultaneously. In our approach, we achieved Treg recruitment that allowed preparation of implantable islets with control on spatiotemporal release of insulin and offer a new level on

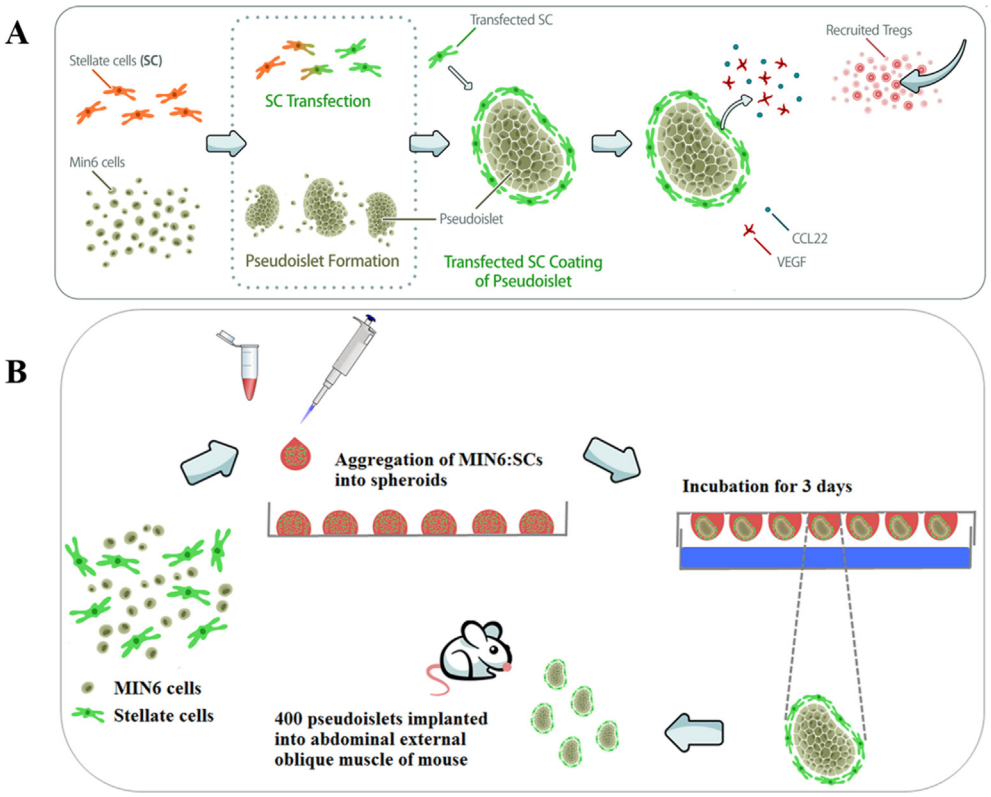

Fig. 1. (A) Preparation of local immune-privileged microenvironment steps through Treg recruitment by the CCL22 protein. **(B)** Schematics of heterospheroid formation by the hanging drop method and implantation into mice. Treg, regulatory T cell.

islet-SC interactions that has not been achieved before. Our results on Treg migration *in vivo* toward transduced and implanted hHSC-MIN6 and hPSC-MIN6 heterospheroids secreting CCL22 suggest that this study will establish a biomimetic microenvironment for transplantable tissues with potential applications ranging from islet transplantation to regenerative medicine.

Results

Morphologically similar pseudoislets were prepared with MIN6 cells and SCs by the hanging drop method

MIN6 β cells were aggregated into spheroids called pseudoislets to mimic naive islet morphology. The hanging drop method was used to prepare MIN6 homospheroids and MIN6:SC heterospheroids. We investigated the effects of initial cell number (300 and 1000), SC type (hHSC and hPSC), and MIN6 to SC (MIN6:SC) cell ratios in the heterospheroid (1:1, 3:1, 5:1, 7:1, 10:1) on the growth and formation of pseudoislets.

To observe MIN6 cells and SCs within the heterospheroid, cells were labeled with two different cell-tracking dyes before spheroid formation and were visualized under a fluorescent microscope (Fig. 2). For all conditions studied, we were able to obtain heterospheroids morphologically similar to real islets by the hanging drop method. Particularly, for the heterospheroid group prepared with 1:1 ratio of MIN6 to SCs, SC cells appeared to occupy a significant fraction of heterospheroid volume. For higher ratios of MIN6 to SCs, higher volume of MIN6 cells were observed within the three-dimensional (3D) heterospheroid structure (Fig. 2).

Viable MIN6:SC pseudoislets were prepared by the hanging drop method

Viability of cells in pseudoislets was assessed by fluorescein diacetate-propidium iodide (FDA-PI) staining assay and visualized under fluorescent microscopy. We obtained a higher percentage of green area than that of red area, indicating the presence of a higher amount of viable cells within heterospheroid structures under all conditions (Fig. 3A and Fig. S1A). We also studied the comparison of 1:1 and 3:1 ratios of MIN6:SC to ensure sufficient amounts of CCL22 secretion from SCs required for local immunosuppression (Fig. 3B and Fig. S1B). For an initial cell number of 300, we obtained similar viability in MIN6:hHSC heterospheroids (92 ± 4% for 1:1 and 91 ± 6% for 3:1 ratios of MIN6:SC) compared to that of MIN6 homospheroids (92 ± 4%). However, slight decreases in viabilities were measured for MIN6:hPSC heterospheroids (86 ± 6% for 1:1 and 83 ± 4% for 3:1 ratios of MIN6:SC). Decreased viabilities were observed in larger pseudoislets than in pseudoislets with smaller diameters. For an initial cell number of 1000, viabilities were measured as 73 ± 6% and 71 ± 15% for 1:1 and 3:1 ratios of MIN6:hPSC heterospheroids, respectively. Interestingly, slightly higher viabilities were measured with MIN6:hHSC heterospheroids (87 ± 4% for both 1:1 and 3:1 ratios of MIN6:hPSC heterospheroids) than with MIN6 homospheroids (83 ± 10%). These observations suggested that hHSCs promoted the viability of pseudoislets, while hPSCs slightly compromised the viability of pseudoislets (Fig. 3B). As expected, spheroids that initially contained 1000 cells as the initial cell number were larger than those with only 300 cells. (Fig. 3C and Fig. S2). For both initial cell numbers of 300 and 1000, MIN6:hHSC heterospheroid and MIN6 homospheroid morphologies were similar. Average diameters of pseudoislets prepared with an initial cell number of 300 and 1:0, 1:1, and 3:1 ratios of MIN6:hHSC heterospheroid were measured as 109.3 μm, 109.8 μm, and 104.4 μm, respectively. We observed significantly larger heterospheroid diameters for MIN6:hPSC and compared these measurements with those of MIN6:hHSC heterospheroids with both initial cell numbers of 300 and 1000. Average diameters measured for MIN6:hPSC heterospheroids with ratios of 1:1 and 3:1 were 128.2 μm and 123.5 μm, respectively. Slightly larger diameters of heterospheroids prepared with hPSCs than that of those prepared with hHSCs could be attributed to the relatively larger sizes of hPSCs than those of hHSCs.

Effects of different types of SCs (hHSC or hPSC) within heterospheroid formation on the metabolic activity of pseudoislets were investigated through the measurement of intracellular ATP. ATP amounts of heterospheroids were normalized with respect to the value of control group (MIN6 homospheroids). For both spheroid sizes, we observed lower levels of ATP in MIN6:hHSC heterospheroids than in MIN6:hPSC heterospheroids (Fig. 3D).

Functionality of pseudoislets were not affected by SCs

Insulin secretion from pseudoislets was analyzed via static incubation of pseudoislets in Krebs-Ringer buffer (KRB) with altered glucose concentrations. Then, stimulation index (SI), which represents the ratio of the amount of insulin secretion at high-glucose medium to the amount of insulin secretion at low-glucose buffer by pseudoislets, was calculated. An SI value of greater than one indicates functional pseudoislets, which can respond to high glucose by secreting more insulin compared to the insulin secretion at low glucose. We observed that MIN6:SC pseudoislets prepared by the hanging drop method were functional and could secrete insulin in response to buffers with altered glucose concentrations (Fig. 3E and F). We observed that pseudoislets prepared with 300 cells in the droplet were more functional and had slightly higher stimulation indices than the pseudoislets prepared with 1000 cells in the droplets. This result may suggest that increasing cell number in the droplet negatively influences insulin secretion from pseudoislets probably because of limited diffusion of nutrients and oxygen toward the cells in the core of pseudoislets. In general, slightly higher stimulation indices were measured with MIN6:hHSC pseudoislets than with MIN6:hPSC pseudoislets, although no significant differences in insulin secretion between homospheroids and heterospheroids were noted.

Viability and functionality of pseudoislets were not affected by transfection of SCs.

hHSCs and hPSCs were transduced by the pBABE retroviral vector, and they were then characterized for CCL22 protein secretion. We characterized both mRNA CCL22 level through real-time reverse transcription-polymerase chain reaction (RT-PCR) (Fig. 4A) and protein expression level from transduced SCs using human CCL22/MDC Quantikine ELISA assay (Fig. 4B). For both hHSCs and hPSCs, significant amounts of mRNA and protein release were measured after SC transduction (Fig. 4).

Because we measured higher viability (Fig. 3B and D) and functionality (Fig. 3E and F) with pseudoislets prepared with 300 cells as the initial cell number in the droplet, we continued subsequent experiments with 300 initial cells in the droplet. We prepared pseudoislets with MIN6 cells and transduced SCs, which can secrete CCL22. We investigated heterospheroid survival with FDA/PI staining assay and visualized fluorescence under a fluorescent microscope (Fig. 5A). We also tested the influence of transduced SCs' incorporation within heterospheroid on pseudoislet survival and calculated the percentage viability of pseudoislets via FDA/PI assay. We observed a higher percentage of green area than that of red area, suggesting a higher number of live cells than dead cells (Fig. 5B and Fig. S4). We obtained similar viabilities with MIN6:hHSC heterospheroids prepared with different cell ratios, where hHSCs were transduced for CCL22 secretion. Heterospheroid viabilities were measured as 96 ± 2% for 1:1 ratio of MIN6:hHSC and 95 ± 1% for 3:1 ratio of MIN6:hHSC heterospheroids, where MIN6-only homospheroids had a viability of 95 ± 2%. Viabilities measured with MIN6:hPSC heterospheroids, where hPSCs were transduced for CCL22 secretion, were also above 90% (93 ± 4% for 1:1 and 90 ± 4% for 3:1 MIN6:hPSC ratios). When we normalized viability of heterospheroids with respect to the viability of MIN6 homospheroids, we measured higher values for MIN6:hHSC heterospheroids than for MIN6:hPSC (Fig. S4). Then, we characterized diameter and area of pseudoislets prepared with transduced SCs and MIN6 and compared these values with that of MIN6-only

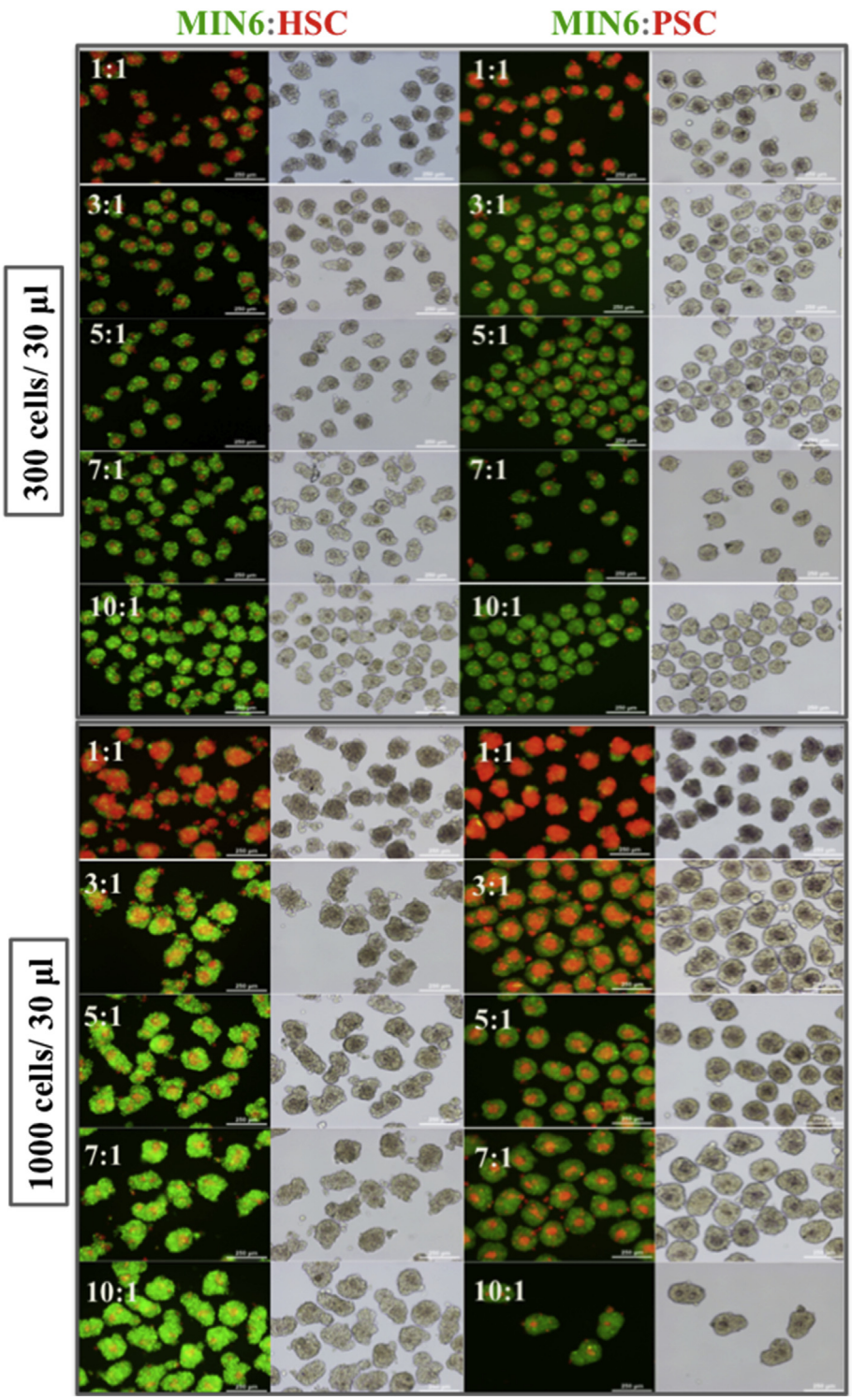

Fig. 2. Distribution of MIN6 cells and SCs within 3D spheroids. Cells were stained with a 5 µM cell tracker dye for 1 h before spheroid formation. Different cell numbers, 300 cells and 1000 cells per 30 µl droplet, and altered MIN6-to-SC ratio (1:1, 3:1, 5:1, 7:1, 10:1) were used for heterospheroid formation. The hanging drop method was used, and cells were incubated within the droplet for 3 days. After 3 days, pseudoislets were visualized and photographed under a fluorescent microscope, n > 3 (MIN6: green; SCs: red) (scale bar: 250 µm).

control group (Fig. 5C and Fig. S5). We obtained similar spheroid sizes formed by aggregation of MIN6 cells and transduced hHSCs or hPSCs. The average diameters were 110 µm for MIN6 homospheroids and 105 µm and 111 µm for 1:1 and 3:1 ratios of MIN6:hHSC, respectively. MIN6:hPSC heterospheroid diameters were measured as 109 µm and 117 µm for 1:1 and 3:1 MIN6:hPSC heterospheroid ratios, respectively. Then, we measured intracellular ATP activity as further evidence for cell viability. We normalized ATP activity of MIN6:SC heterospheroids with respect to MIN6 homospheroids. Intracellular ATP activities for CCL22-transduced SC heterospheroids, prepared with either hPSC or hHSC, were similar to the values measured for MIN6-only homospheroids (Fig. 5D).

Then, we measured insulin secretion from MIN6:SC-CCL22 heterospheroids in response to low and high glucose concentrations and calculated SI to evaluate functionality of pseudoislets (Fig. 5E). We normalized stimulation indices of MIN6:SC heterospheroids with respect to MIN6 homospheroids and confirmed the functionality of heterospheroids. This finding suggested that incorporation of transduced hHSCs or hPSCs that secrete CCL22 within a heterospheroid prepared with MIN6 cells did not compromise the functionality of MIN6 cells.

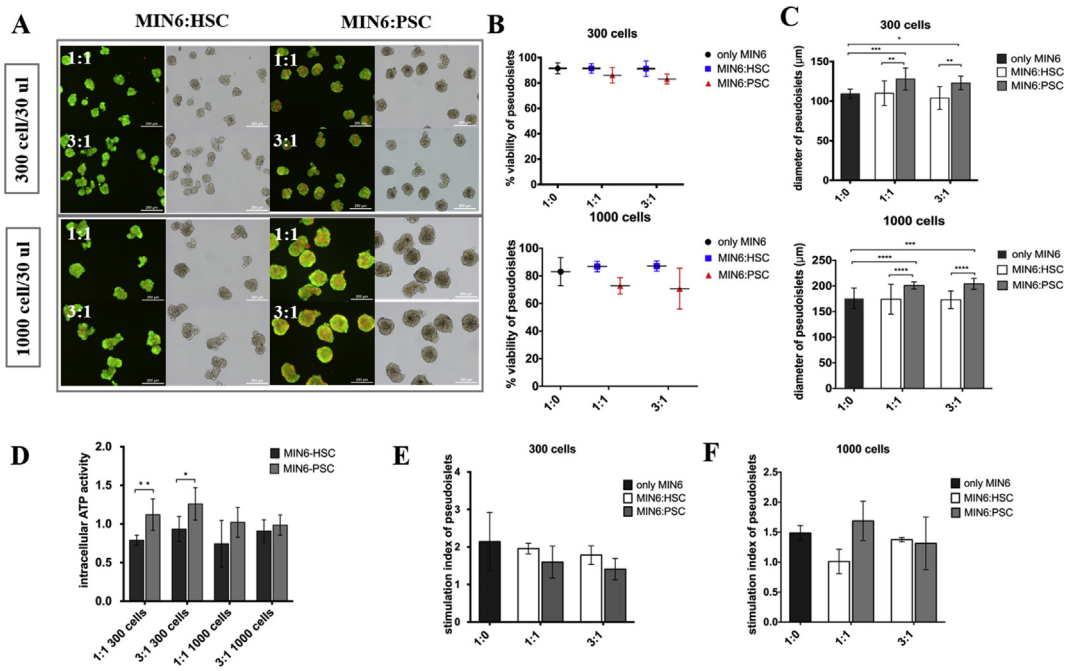

Fig. 3. Viability and morphology of pseudoislets by FDA-PI staining. (A) Live cells were stained green using FDA , and dead cells were stained red using PI and then photographed under a fluorescent microscope. Initial cell numbers of 300 and 1000 cells per 30 μl and different cell ratios (1:1, 3:1) of MIN6:SCs were used for spheroid formation (scale bar: 250 μm). (B) Viability and (C) diameter were calculated using ImageJ software (n > 3). (D) Intracellular ATP activity of pseudoislets with different initial cell numbers and types of SCs. Both cell survival rates in heterospheroids were normalized with respect to homospheroid, and the statistical significance was compared to the homospheroid control group (n = 3). (E, F) Insulin secretion from MIN6:SC (1:1, 3:1) pseudoislets in response to glucose. Pseudoislets were incubated in low-glucose (2.8 mM) and high-glucose (28 mM) solutions for 1 h each. Then, supernatants were collected and analyzed by Insulin ELISA. SI was calculated as the ratio of insulin secretion at high glucose to the value of insulin at low glucose for both sizes of pseudoislets; 300 cells (E) and 1000 cells (F) (n = 3). All data are represented as mean ± SD. **** $p < 0.0001$, *** $p < 0.001$, ** $p < 0.01$, and * $p < 0.05$. FDA-PI, fluorescein diacetate-propidium iodide; SI, stimulation index; SD, standard deviation.

Secretion of CCL22 from pseudoislets can recruit Tregs toward the implantation site in vivo

To ensure recruitment of Tregs due to CCL22 secretion from transduced SCs, we carried out *in vivo* experiments with both non-diabetic and diabetic animal models. To ensure sufficient amount of CCL22 expression by SC and Treg recruitment, we carried out *in vivo* experiments with 1:1 MIN6-to-SC ratio (Fig. 6A and B). *In vivo* experiments were carried out with non-diabetic or diabetic male $CD1^+$ mice where experimental groups are described in Table S1. Abdominal external oblique muscle was chosen as the implantation site for both non-diabetic and diabetic animal models. It has been demonstrated that abdominal external oblique muscle is a promising site for islet transplantation because it provides vascularization and non-invasive operation because of its accessibility [42]. Twenty days

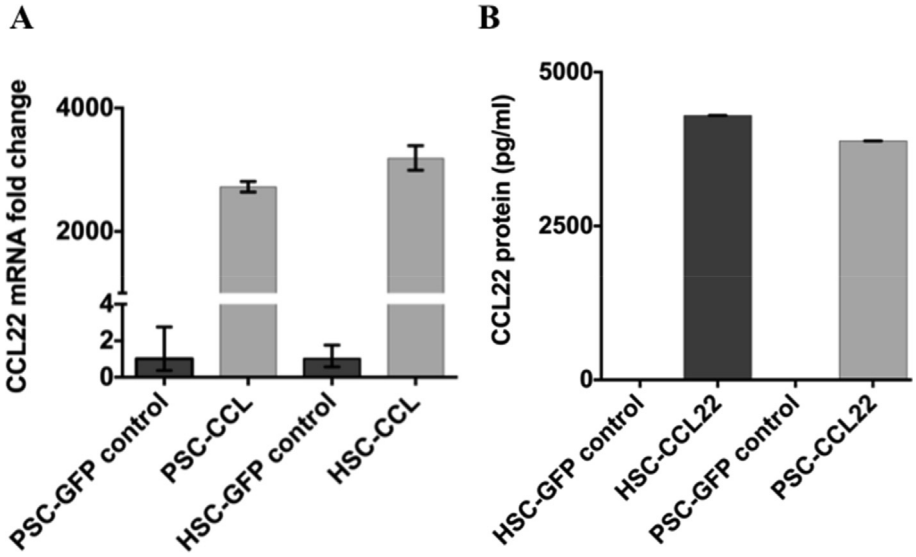

Fig. 4. CCL22 expression by transduced SCs. They were transfected with retroviral pBABE-CCL22 or pBABE-green fluorescent protein (GFP) as the control. (A) CCL22 mRNA levels in transfected SCs were analyzed by quantitative polymerase chain reaction (qPCR) and CCL22 expression was normalized to GAPDH (control gene) (n = 3). (B) CCL22 protein expression by transduced SCs was determined by CCL22 ELISA.

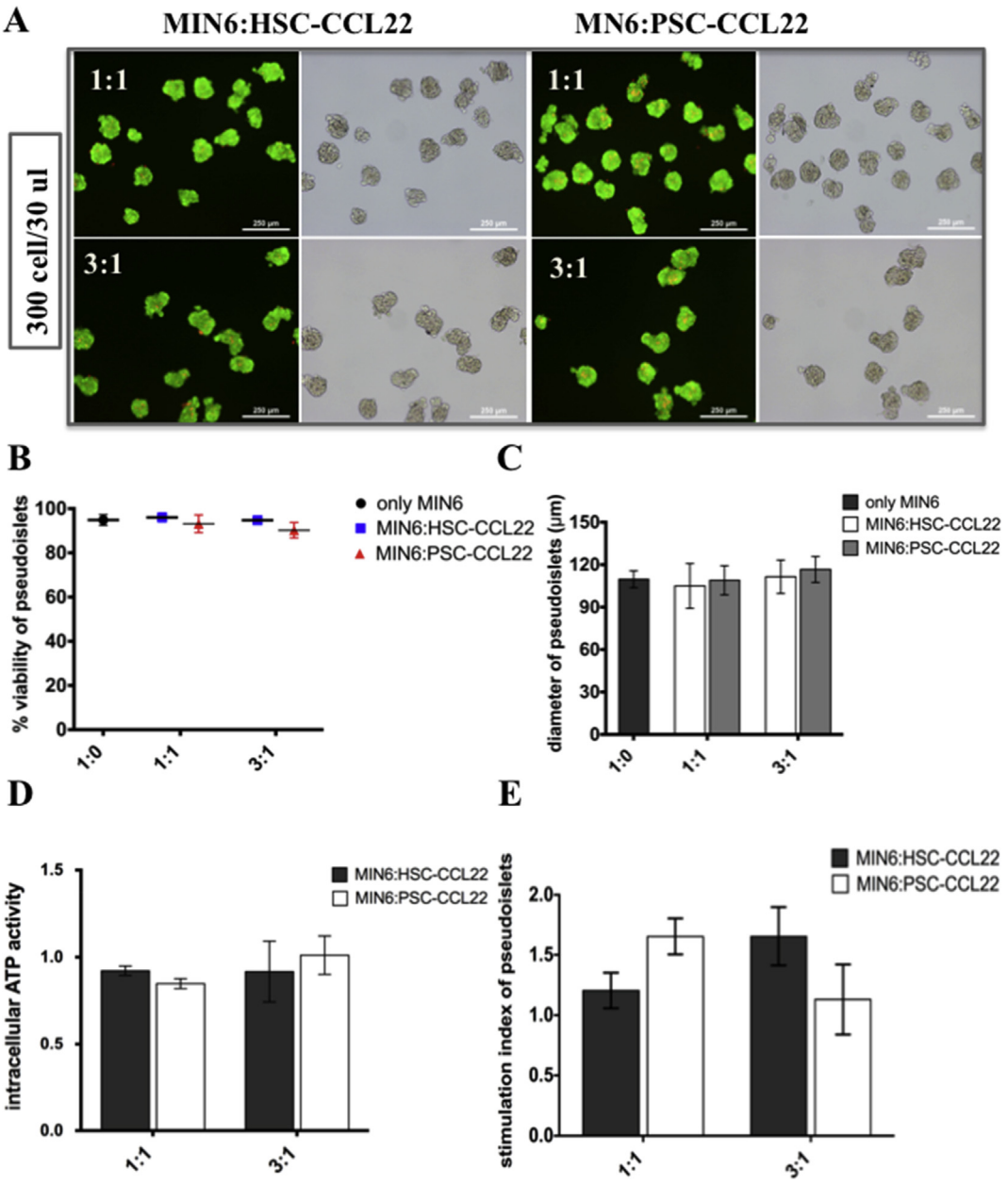

Fig. 5. Viability, morphology, and functionality of pseudoislets containing MIN6 cells and transduced SCs. (A) Live cells were stained green using FDA, and dead cells were stained red using PI red and then examined and photographed under a fluorescent microscope. (B) Percentage of viable cells in pseudoislets and (C) diameter of pseudoislets were calculated using ImageJ. (D) Intracellular ATP activity of heterospheroids was also calculated. SI was calculated as the ratio of insulin secretion at high glucose to the value of insulin at low glucose. (E) The initial cell number was 300 cells per 30 μl. Cell ratios of MIN6 to SCs were 1:1 and 3:1 ($n > 3$) (scale bar: 250 μm). Scs, stellate cells; Tregs, regulatory T cells, SI, stimulation index; FDA, fluorescein diacetate; PI, propidium iodide.

after transplantation, tissues from non-diabetic recipient mice were retrieved and analyzed using a flow cytometer. After analysis of tissue, higher Treg population was measured in MIN6:hHSC pseudoislets secreting CCL22 than in the other groups (Fig. S6). A higher amount of Treg recruitment toward the implantation site by the heterospheroids prepared with MIN6 cells and transduced hHSC cells suggested that transduced hHSCs could secrete CCL22 *in vivo* and promote recruitment of Tregs toward the implantation site in the non-diabetic animal model. To further elucidate the capability of Treg recruitment with the diabetic mouse model, we carried out a second set of *in vivo* experiments with diabetic mice. We chose MIN6:hHSC-CCL22 pseudoislets for experiments with the diabetic model because there was a slight increase in Treg recruitment compared with MIN6:hPSC-CCL22. Pseudoislets were implanted to the left abdominal external oblique muscle as the implantation site, and no implantation was performed at the right abdominal external oblique muscle as the control site. For each animal, tissues from both implantation site and control site were retrieved 10 days after transplantation and analyzed using a flow cytometer. Similarly, in the presence of MIN6:hHSC-CCL22 heterospheroids, we observed a higher amount of Treg population than the other groups (Fig. 6B and Fig. S7). In addition, when we compared Treg populations between the tissues from the control site and implantation site, in the MIN6:HSC-CCL22 group, we found that Tregs were selectively recruited to the graft site, where a sevenfold increase in Treg population was observed (Fig. 6C).

Furthermore, we performed implantation of pseudoislets that were prepared with untransduced HSCs and MIN6 cells into non-diabetic

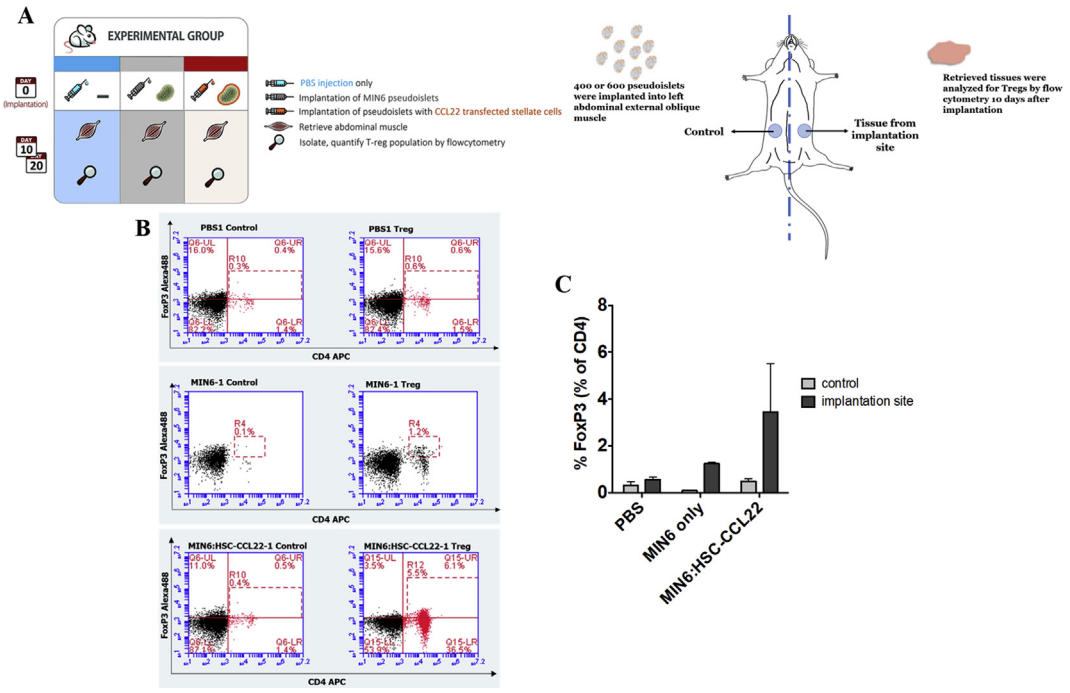

Fig. 6. **(A)** *In vivo* experimental plan and schematics for the demonstrations of implantation sites (external oblique muscle) for the control and experimental groups. **(B)** Recruitment of Tregs *in vivo*. Pseudoislets were implanted into the abdominal external oblique muscle of a diabetic male $CD1^{+}$ mouse. Tissue was retrieved 10 days after transplantation and recruitment of Tregs was confirmed using a flow cytometer for $CD4^{+}CD25$ + FoxP3+ cells. **(C)** Percentage of $FoxP3^{+}$ cells in the $CD4^{+}$ cell population indicates the presence of Tregs in the graft. n = 3 per group. Mean ± SEM. SEM, standard error of mean.

animals. After retrieval of the implanted tissue after 20 days, we carried out hematoxylin and eosin (H&E) staining on both implanted tissue (left abdominal external oblique muscle) and control tissue (right abdominal external oblique muscle). The images that we obtained from H&E staining are presented in Fig. 7. According to this histological analysis, we observed the integrity of the tissue at the control site (Fig. 7A), and we confirmed the presence of our implanted pseudoislets as were shown in the figure (Fig. 7B).

Discussion

The development of tolerance induction approaches via immune engineering that can restore and/or replace non-functional tissues with organ/tissue transplantation represents the leading front of emerging therapies [9,43,44]. Transplantation of pancreatic islets is a promising approach for the treatment of T1D; however, it is still limited by the factors such as the limited number of appropriate donors and requirement of systemic immunosuppressive drugs to prevent graft rejection [1]. Therefore, there is an increasing unmet need for transplantable islets, which are mostly isolated from brain-dead patients [45]. However, viability and functionality of these pancreatic islets are unfavorably affected by brain death [46]. Thus, there is an urgent need for the development of transplantable pseudoislets that can mimic the function of naive islets for the treatment of T1D. In this study, we prepared insulin-secreting pseudoislets through aggregation of MIN6 cells and SCs as a model and mimicked naive islet morphology to address challenges associated with the requirement of high islet numbers and repeated islet isolations. Furthermore, we designed an immune-privileged and special microenvironment around implantable islets to provide graft tolerance through overexpression of CCL22 by SCs.

Previous studies demonstrated that HSCs could regulate the immune system through expanding Tregs and inhibiting T cell responses *in vivo* [30,31,47]. It was also observed that cotransplantation of islets with HSCs protected islet grafts from rejection via forming an immune barrier, such as inhibition of T cells or recruitment of Tregs [32,48]. However, few other studies reported negative influences of PSCs on the function of pancreatic β cells. According to these findings, coculture of PSCs with mouse islets or RIN5F rat pancreatic β cells compromised insulin expression and promoted apoptosis [38,39]. In our study, we developed pseudoislets comprising SCs and MIN6 cells as a unique model and examined distribution of MIN6 and SCs within pseudoislets using different parameters, such as different SC sources (pancreas and liver), initial cell numbers (300 and 1000), and ratios of MIN6 to SC (1:1, 3:1, 5:1, 7:1, and 10:1) (Fig. 2).

We focused on the immunomodulatory potential of both transduced hPSCs and hHSCs to create a locally immune-privileged implantation site so that clinically transplantable islets could be developed without the requirement of immunosuppressive drugs. We chose 1:1 and 3:1 MIN6-to-SC cell ratio to compare the impact of varying amounts of CCL22 secretion by transduced SCs. We also compared the effects of incorporation of both hHSCs and hPSCs on the viability and functionality of MIN6 cells within heterospheroids. For all MIN6 and SC ratios studied, we observed that smaller pseudoislets had higher viability than larger ones (Fig. 3A and B). This is probably due to the limited diffusion of oxygen and nutrients into spheroids and accumulated waste products within spheroids, which lead to subsequent cell death. MIN6 homospheroid survival was measured to be 92 ± 4% when 300 cells were used as the initial cell number during heterospheroid formation via the hanging drop method, whereas cell survival was reduced to 83 ± 10% when 1000 cells were used in the droplet.

Previous islet transplantation studies proved that small islets within a diameter range of 50–100 μm were ideal for successful transplantation because of minimum hypoxia, whereas islets within a diameter range of 100–300 μm suffered from poor nutrient transport [41,49,50]. The real islets range between 50 and 400 μm, with an average diameter of 150 μm [50]. Hence, we prepared heterospheroids with an initial cell number of 300 cells within the droplet during the hanging drop experiments, which yielded an average pseudoislet diameter of 116.5 μm (Fig. 3C). We continued subsequent experiments with similar conditions and obtained heterospheroid diameters within the range of 104–128 μm.

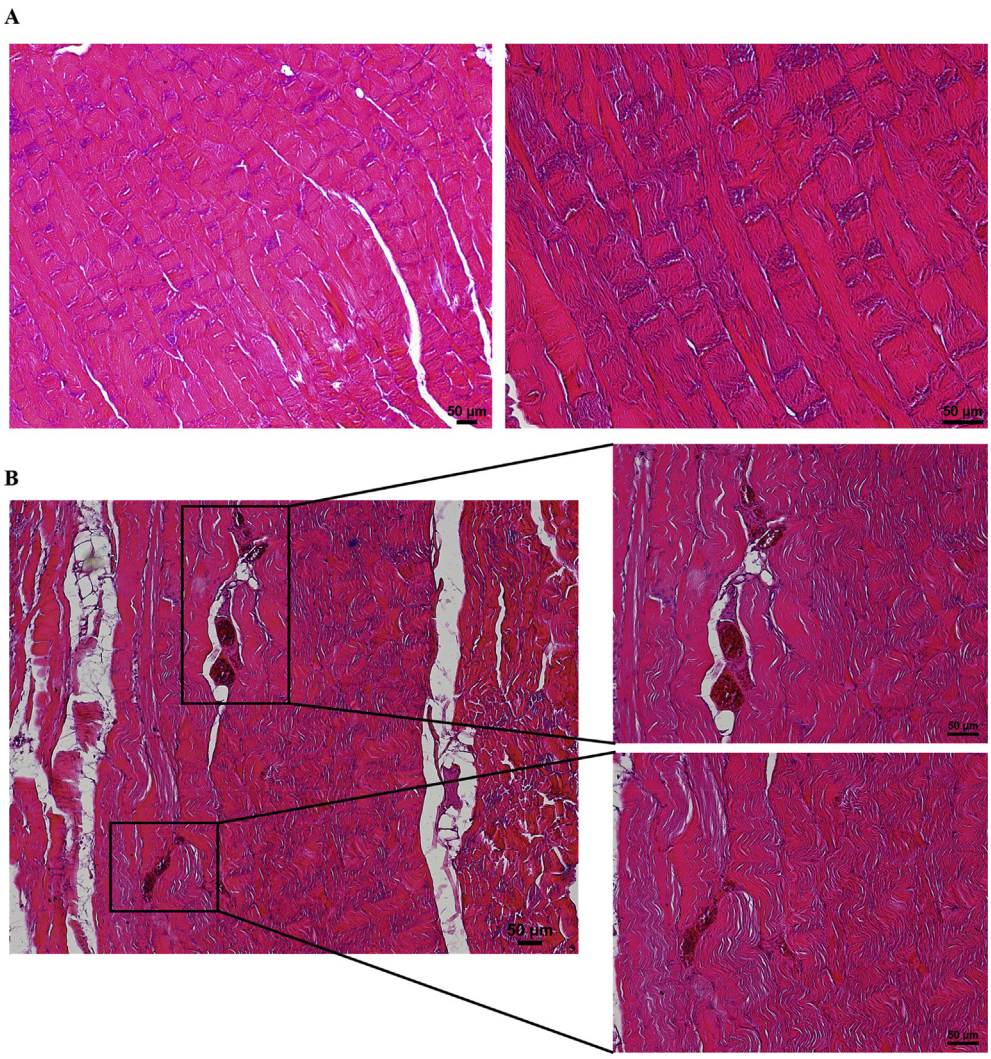

Fig. 7. Histological analysis of tissue obtained from both (A) control site and (B) implantation site in *in vivo* experiments. Tissue sections were stained with hematoxylin and eosin (H&E).

To distinguish the influence of SC type on viability, we prepared heterospheroids with both hPSCs and hHSCs. We observed slight decreases in the survival of pseudoislets when hPSCs were incorporated within the heterospheroids. Interestingly, hHSCs slightly promoted the survival of pseudoislets (Fig. 3B and Fig. S1B). With 300 initial cells in the droplets of hanging drop experiments, we measured slightly lower viabilities when spheroids were prepared with hPSCs, whereas viabilities were higher when hHSCs were used. Previous studies have also reported negative influences of hPSCs on the viability of mouse islets or RIN5F cells, although the comparison of hHSCs and hPSCs on viability has not been investigated before [38,39]. On the other hand, we found significantly higher intracellular ATP levels for MIN6:hPSC heterospheroids (Fig. 3D). Intracellular ATP activity indicates metabolic activity and hence the presence of viable cells. We obtained larger pseudoislets with hPSCs than with hHSCs (Fig. 3C and Fig. S2). The large size of heterospheroids prepared with hPSCs might be the reason for high ATP levels. Previous studies demonstrated that hPSCs would compromise insulin secretion and viability of islets [38,39]. In the present study, we did not observe significant reduction of insulin secretion from heterospheroids (MIN6:hHSCs and MIN6:hPSCs) compared with homospheroids, although there were slight decreases in the SI of MIN6:hPSC heterospheroids (Fig. 3E and F). We also observed that MIN6:hHSC heterospheroids were morphologically similar to MIN6 homospheroids and that they had slightly higher viability than MIN6:hPSC heterospheroids.

Secretion of CCL22 from cancer cells enables them to escape from the immune system. Recently, CCL22-based recruitment of Tregs to the islet graft site has been considered to protect β cells from autoimmune attack, and long-term protection of islet allografts from rejection was achieved by implantation of CCL22 plasmid *in vivo*. CCL22 binds to the CCR4 receptor on Tregs, and this receptor is also found on the membrane of other immune cell subsets involved in immunosuppression, suggesting that our strategy has the potential for recruitment of other immunosuppressive cells such as invariant natural killer T (iNKT) cells and plasmacytoid dendritic cells (pDCs) which are key players in attenuating local autoimmunity around the graft [42]. It has been demonstrated that release of CCL22 around islet grafts from polymeric particles could prevent immune attack of islet grafts and attenuate T1D through Treg recruitment [51–54].

In this study, SCs were transduced by a retroviral vector to express CCL22 protein, and CCL22 overexpression was verified at mRNA and protein levels (Fig. 4). The influence of transduced SCs and secretion of CCL22 on the viability of heterospheroids were investigated in detail. We obtained similar effects of transduced and untransduced SCs on the morphology, viability, and functionality of heterospheroids (Fig. 5 and Fig. S3). Average viability of CCL22-secreting MIN6:hHSC heterospheroids was found to be slightly higher than that of CCL22-secreting

MIN6:hPSC heterospheroids. Viability of MIN6 homospheroids was around 95 ± 2% which was similar to that of CCL22-secreting MIN6:hHSC heterospheroids. These findings suggested that transduction of SCs and CCL22 secretion from pseudoislets did not adversely affect morphology and viability of heterospheroids.

To distinguish the effects of transduced hPSCs and hHSCs on Treg recruitment, we performed *in vivo* experiments in non-diabetic animals. For these experiments, we implanted pseudoislets into the external abdominal oblique muscle of non-diabetic $CD1^+$ mice. We measured the population of Tregs around the graft site on day 20. As expected, we observed a higher percentage of Tregs around the graft that included CCL22-secreting MIN6:hHSC heterospheroids than the other groups after the retrieval of the tissue on day 20 (Fig. S6). Percentage of $FoxP3^+$ cells in the $CD4^+$ cell population indicates the presence of $CD4^+CD25^+FoxP3^+$ Tregs expressing CCR4 which is the receptor for CCL22 chemokine secreted from the graft [51,52]. To test the efficacy of our model for the recruitment of Tregs toward the implantation site in a diabetic mice model, we transplanted 600 pseudoislets into the left external abdominal oblique muscle of streptozotocin (STZ)-induced diabetic $CD1^+$ mice. Ten days after implantation, tissues were retrieved and Treg recruitment to the implantation site was measured. Consistent with the non-diabetic animal model experiments, we found an increased number of Treg population at the implantation site that included hHSC-CCL22 cells, which strongly suggested selective recruitment of Tregs toward the implantation site (Fig. 6B–C and Fig. S7).

Furthermore, we performed additional *in vivo* experiments in non-diabetic mice with pseudoislets composed of MIN6 and untransduced HSCs (MIN6:HSC pseudoislets), which were used as a control for the transfection step. Tissues from both control and implantation site were retrieved 20 days after implantation, and Treg population was measured using a flow cytometer. We did not observe any difference in Treg population between control and experimental groups (Fig. S8). This suggested that CCL22 secretion from transduced SCs is crucial for efficient Treg recruitment toward the implantation site.

Tregs have been usually detected with low numbers in peripheral blood. Typical range of Tregs in $CD4^+$ T-cell population is 4–9% [30,35]. We managed to recruit 5.5% Tregs toward the implantation site with the group MIN6:HSC-CCL22, which is within the typical range of Treg population in all $CD4^+$ cells (Fig. 6B). It is known that the function and development of Tregs are strongly dependent on the transcription factor FoxP3 expression [55]. However, under certain immunological conditions, $FoxP3^+$ Tregs might be unstable and lose FoxP3 expression [56]. For example, in a previous study, it was suggested that Tregs isolated from inflammatory sites have lower FoxP3 expression and an autoimmune microenvironment such as T1D causes loss of FoxP3 expression in Tregs [57]. Therefore, the possible reason for the difference in Treg frequency between diabetic and non-diabetic animals is alteration in the FoxP3 expression, which is also a known immunophenotype for T1D [58]. In this study, we observed a higher trend of Treg recruitment with MIN6:HSC-CCL22 pseudoislets in a diabetic animal model *in vivo* (Fig. 6C).

Finally, we implanted pseudoislets that were prepared with untransduced HSCs and MIN6 cells into non-diabetic animals, where we observed integrity of the tissue at the control site and confirmed the presence of implanted pseudoislets (Fig. 7A and B). According to the results of H&E analysis, 20 days after implantation, pseudoislets remained at the implantation site and reserved their integrity. Furthermore, no inflammatory response was observed because no macrophages and immune cells were visible at the implantation site.

These observations suggested that our heterospheroid pseudoislet model system incorporating insulin-secreting MIN6 cells and transduced SCs were capable of recruiting Tregs to graft a microenvironment in both non-diabetic and diabetic animal models.

With this report, we present for the first time evidence of a unique model that incorporates MIN6 cells and transduced human SCs within a heterospheroid structure where transduced SCs could secrete CCL22 and recruit Tregs toward the implantation site *in vivo*. Manipulating immune cell trafficking via CCL22 gene therapy and harnessing SCs is a unique therapeutic approach not only for the treatment of T1D but also for other chronic diseases such as anemia, cancer, and central nervous system (CNS) disorders which might involve cell transplantation and hence immune modulation through Treg recruitment toward the implantation site.

Conclusions

We developed a heterospheroid model and investigated the effects of both pancreatic and hepatic types of SCs on the viability and functionality of MIN6 cells both *in vitro* and *in vivo*. We designed a locally immune-privileged site around the graft and achieved Treg migration toward the graft. SCs were transduced to express chemokine CCL22, a chemokine secreted from cancer cells to evade immune destruction through specific recruitment of Tregs. Viable and functional pseudoislet heterospheroids were prepared with MIN6 and SCs by the hanging drop method. We observed that transduction of SCs to express CCL22 did not compromise viability and functionality of pseudoislets and that this model system could promote the recruitment of Tregs toward the implantation site. SCs have excellent angiogenesis promotion capabilities also, thereby making this strategy even more attractive and promising for clinical translation to provide a way to transplantable tissues with vascularization potential and without the use of immunosuppressive drugs. Furthermore, the strategy of promoting Treg migration and vascularization around the graft site will be a desirable therapeutic approach for the treatment of T1D through islet transplantation. This study is promising to provide a fundamental understanding of the SC-islet interaction and ligand synthesis and transport from SCs at the graft site for ensuring local immune tolerance to target T1D. Our results may also establish a new paradigm for creating tolerable grafts for other chronic diseases such as diabetes, anemia, and CNS diseases and advance the science of graft tolerance.

Experimental procedures

Cell culture

Human pancreatic stellate cells (hPSCs) and human hepatic stellate cells (hHSCs) were isolated and cultivated at Koc University Hospital according to previously published protocols with minor modifications [59,60]. The study protocol was approved by the Koç University Clinical Research Ethics Committee and the local institutional review board (2015.167.IRB2.064). SCs were maintained in Dulbecco's Modified Eagle Medium (DMEM) Nutrient Mixture F-12 (DMEM:F12; Gibco) supplemented with 10% fetal bovine serum (FBS) (heat inactivated; Gibco) and 1% penicillin-streptomycin (Sigma) and incubated at 37 °C under 5% CO_2 environment. MIN6 cells were provided by the Dr. Donald F. Steiner's Laboratory at the University of Chicago. MIN6 cells were cultured in DMEM (HG; Gibco), 10% FBS, 1% L-glutamine (Sigma), 1% sodium pyruvate (Lonza), 1% penicillin-streptomycin (Sigma), and 100 nM β-mercaptoethanol (Gibco) and incubated at 37 °C in a humidified 5% CO_2 incubator. Hek293T cells (ATCC) (up to passage 10) were cultured in DMEM (Gibco) with 10% FBS and 1% penicillin-streptomycin and incubated at 37 °C and 5% CO_2 for transfection experiments.

Plasmid constructs, virus production, and infection of hPSCs

pBABE-GFP plasmid was a gift from Prof. Tamer Onder at Koc University. pCMV6-AC plasmid including human CCL22 gene (Origene) was used as a template for PCR-based cloning, and CCL22 gene was cloned by flanking *Bam*HI and *Sal*I cut sites into the retroviral pBabe-puro (Addgene) mammalian expression vector. Retrovirus was produced by cotransfection of HEK293 cells with the CCL22 vector and other vectors: packaging plasmid (pUMVC) and envelope glycoprotein of the vesicular stomatitis virus (VSVG) as described [61]. Viruses were 100×

concentrated using 50% (w/v) polyethylene glycol (PEG) solution. SCs were seeded in a 96 well plate at a density of 10^5 cells/well. The next day, cells were infected with retroviruses (GFP or CCL22) containing 10 μg/ml of protamine sulfate (PS) and incubated for 2 days at 37 °C and 5% CO_2. Double infection was performed to enhance the transduction efficiency. SCs were selected by adding puromycin at a final concentration of 2 μg/ml for 3 days.

qRT-PCR

Total RNA was extracted using an RNA extraction kit from Macherey-Nagel according to the manufacturer's instructions. cDNA was synthesized by using Moloney murine leukemia virus reverse transcriptase (M-MLV RT; Invitrogen). Relative gene expression levels of CCL22 were detected using LightCycler® 480 SYBR Green I Master (Roche). Relative quantification of gene expression was performed using GAPDH as a housekeeping gene. real-time reverse transcription-polymerase chain reaction (qRT-PCRs) was carried out using the primers listed in Table S2. Gene expression levels were calculated by 2-ΔΔCt method.

CCL22 protein determination

Transduced SCs (9×10^4) were seeded on a 6-cm Petri dish, and the medium was refreshed after day 2. Then, the medium was collected on day 5 after seeding, and secreted CCL22 protein levels in serum were characterized using Human Quantikine CCL22 ELISA kit (R&D Systems) following the manufacturer's instructions.

Cell Tracker dye staining and heterospheroid formation by the hanging drop method

The hanging drop technique was used to prepare pseudoislets by agglomerating MIN6 or MIN6:SC cells into spheroids (Fig. 1B). To monitor cell distribution of MIN6 and SCs within heterospheroids, SCs were stained with 5 μM Cell Tracker red (Invitrogen) and MIN6 cells were stained with 5 μM Cell tracker green (Invitrogen) for 1 h before spheroid formation. Different cell densities, 300 and 1000 cells per 30 μl, were prepared for MIN6 homospheroid and MIN6:SC heterospheroid formation. For heterospheroid formation, MIN6 and SCs cell suspensions were prepared at ratios of 1:1, 3:1, 5:1, 7:1, and 10:1 (MIN6 to SCs). The medium was prepared by using DMEM:F12 and DMEM, 50% by volume from each, without β mercaptoethanol. Thirty microliters of cell suspension was pipetted onto the inner surface of Petri dish lids (diameter = 10 cm), and inverted lids were placed on top of the dishes containing 8 ml of phosphate-buffered saline (PBS) with 1% penicillin-streptomycin. Droplets were incubated at an inverted position for 3 days at 37 °C and 5% CO_2.

Live/dead cell staining of pseudoislets

The viability of pseudoislets was characterized by an inclusion dye, FDA, and an exclusion dye, PI, staining. Pseudoislets prepared through the hanging drop method were transferred to PBS. Pseudoislets were stained with 8.5 μg/ml of PI and 42.4 ng/ml of FDA. After 5 min of incubation in the dark, islets were washed with PBS and then visualized and imaged by fluorescent microscopy. Viable cells were stained green, and dead cells were stained red. The percentage of viable cells and area of pseudoislets were estimated using ImageJ. The mean and standard deviation of viable cell numbers were also calculated.

Metabolic activity of pseudoislets

Intracellular ATP activity of pseudoislets was measured by CellTiter Glo (Promega) assay. Briefly, 15 pseudoislets prepared through the hanging drop method were hand-picked, collected in 120 μl of cell culture medium, and transferred to a 96-well plate. Then, 60 μl of each reagent was added to each well. The cell culture medium was prepared with MIN6 β-mercaptoethanol free growth medium and SCs growth medium, where 50% v/v was used from each medium. Islets were incubated at 200 rpm for 15 min under dark for the analysis of ATP activity. The ATP activity was measured on a microplate reader (Synergy H1 Hybrid Multi-Mode Microplate Reader; Bio-Tek).

Insulin secretion function of pseudoislets

Insulin secretion from pseudoislets in response to altered glucose buffers was measured by static incubation assay. Briefly, 20 pseudoislets were hand-picked and plated on a cell culture insert (12 μm) in 1 ml of KRB containing 2.8 mM glucose (low glucose) and incubated for 1 h to bring insulin secretion to the baseline level. Then, incubation of pseudoislets in fresh low-glucose buffer medium was repeated, and supernatant from the medium was collected. Inserts containing pseudoislets were transferred to 1 ml of high-glucose KRB containing 28 mM glucose (high glucose) and incubated for 1 h. KRB media were collected and stored at −20 °C until further characterization of insulin. Insulin was measured using a mouse insulin ELISA kit (Mercodia) as per the manufacturer's instructions. To quantify insulin release, SI was calculated as the ratio of insulin secretion at high-glucose to the insulin secretion at low-glucose buffer as follows:

$$stimulation\ index = \frac{amount\ of\ insulin\ secreted\ at\ high\ glucose}{amount\ of\ insulin\ secreted\ at\ low\ glucose} \quad (1)$$

In vivo implantation of pseudoislets

All *in vivo* experiments were approved by the institution review boards of Koc University (HADYEK). Non-diabetic and diabetic male CD1 mice were used and maintained in conventional housing at the Koç University Animal Research Facility (KUARF) for *in vivo* experiments. For non-diabetic group experiments, male CD1 mice (aged 8–9 weeks) weighing 19–24 g were used and maintained in conventional housing at the KUARF for in *vivo* experiments. MIN6:SC heterospheroid pseudoislets (400) secreting CCL22 prepared by the hanging drop method were implanted into the abdominal external oblique muscle of the recipient mouse. Twenty days after transplantation, tissues from recipient mice were retrieved and analyzed using a flow cytometer (Fig. 6A).

For diabetic group experiments, male CD1 mice weighing 28–33 g were used, and they received intraperitoneal injection of STZ (AdipoGen) at a dose of 50 mg/kg body weight for five consecutive days. After STZ injection, animals were monitored for fasting blood glucose levels. Blood glucose was measured using an Accu-Chek glucose meter from the tail vein. Mice with a blood glucose level higher than 300 mg/dl were considered as diabetic and used for the transplantation experiments (Fig. S9). For these experiments, three groups have been used: (1) animals in group one received only PBS injections, (2) animals in group two received MIN6 homospheroids, and (3) animals in group three received MIN6:hHSC-CCL22 heterospheroids (Table S1). Homospheroids/heterospheroids or PBS is implanted into the left abdominal external oblique muscle of diabetic mice and maintained for 10 days. The right abdominal external oblique muscle was retrieved as the control tissue. Body weight of the transplanted mice was monitored at regular intervals. Tissues of same weight from both left abdominal external oblique muscle (implantation site) and right abdominal external oblique muscle (control) were surgically removed from mice 10 days after transplantation and analyzed using a flow cytometer.

Flow cytometry

Tissues from both implantation site and control site were retrieved 10 days after transplantation and analyzed for Treg recruitment. Briefly,

cells were isolated from tissues by mechanically disrupting the tissue in a serum-free RPMI medium and passed through 70-μm strainers to dissociate the aggregates into a single cell suspension. Cells were counted and adjusted to a maximum of 10,000 cells/μl. $CD4^{+}FoxP3^{+}$ Tregs in tissues were detected using a True-Nuclear FoxP3 Mouse T-Reg Flow Kit (Biolegend) according to the manufacturer's instructions.

Histological analysis

Tissues from both implantation (left) and control site (right) were retrieved 20 days after implantation, immediately fixed in 10% formalin, and embedded in paraffin. Tissues were sectioned at a thickness of 7 μm. Tissue sections were stained with H&E stain for histological examination. Sections were visualized and imaged by bright field microscopy.

Statistical analysis

Statistical analysis was performed using Graph Pad Prism 6 software. Methods used to report the results are mentioned in the figure legends. Multiple comparisons between groups were analyzed by two-way analysis of variance followed by Tukey's post hoc testing; $p < 0.05$ was considered statistically significant.

Author contribution

D.C.O., M.B.A., Y.I., T.L., O.A., and T.B. performed or participated in data acquisition and analysis. D.C.O, M.B.A., and Y.I. wrote the manuscript. M.K. and M.E. provided human stellate cells. T.B.O. assisted with molecular cloning, and F.C. assisted with flow cytometer sample processing and data acquirement. S.K. conceived the study, designed the experiments, wrote the manuscript, and provided funding for the study.

Acknowledgments

This study is supported by the Scientific and Technological Research Council of Turkey (TUBITAK) under 1001-Scientific and Technological Research Projects Funding Program (SBAG 116S442) and Koç University Seed Fund SF.00028. The authors thank Dr. Ali Cihan Taşkın, Ahmet Kocabay, and Nihan Coşkun from the Koç University Animal Research Facility (KUARF) for *in vivo* experiments. The authors gratefully acknowledge the use of the services and facilities of the Koç University Research Center for Translational Medicine (KUTTAM), funded by the Presidency of Turkey, Presidency of Strategy and Budget. The content is solely the responsibility of the authors and does not necessarily represent the official views of the Presidency of Strategy and Budget.

Conflict of interests

The authors declare that they have no known competing financial interests or personal relationships that could have appeared to influence the work reported in this paper.

Appendix A. Supplementary data

Supplementary data to this article can be found online at https://doi.org/10.1016/j.mtbio.2019.100006.

References

[1] B. Kepsutlu, C. Nazli, T. Bal, S. Kizilel, Design of bioartificial pancreas with functional micro/nano-based encapsulation of islets, Curr. Pharmaceut. Biotechnol. 15 (2014) 590–608.
[2] S. Kizilel, M. Garfinkel, E. Opara, The bioartificial pancreas: progress and challenges, Diabetes Technol. Ther. 7 (2005) 968–985.
[3] T. Bal, C. Nazli, A. Okcu, G. Duruksu, E. Karaoz, S. Kizilel, Mesenchymal stem cells and ligand incorporation in biomimetic poly(ethylene glycol) hydrogels significantly improve insulin secretion from pancreatic islets, J. Tissue Eng. Regenerat. Med. 11 (2017) 694–703.
[4] T. Bal, D.C. Oran, Y. Sasaki, K. Akiyoshi, S. Kizilel, Sequential coating of insulin secreting beta cells within multilayers of polysaccharide nanogels, Macromol. Biosci. 18 (2018), e1800001.
[5] M.G. Roncarolo, M. Battaglia, Regulatory T-cell immunotherapy for tolerance to self antigens and alloantigens in humans, Nat. Rev. Immunol. 7 (2007) 585–598.
[6] C. Ferretti, A. La Cava, Adaptive immune regulation in autoimmune diabetes, Autoimmun. Rev. 15 (2016) 236–241.
[7] R.F. Gibly, J.G. Graham, X. Luo, W.L. Lowe Jr., B.J. Hering, L.D. Shea, Advancing islet transplantation: from engraftment to the immune response, Diabetologia 54 (2011) 2494–2505.
[8] X. Luo, S.D. Miller, L.D. Shea, Immune tolerance for autoimmune disease and cell transplantation, Annu. Rev. Biomed. Eng. 18 (2016) 181–205.
[9] T.T. Jiang, T. Martinov, L. Xin, J.M. Kinder, J.A. Spanier, B.T. Fife, et al., Programmed death-1 culls peripheral accumulation of high-affinity autoreactive CD4 T cells to protect against autoimmunity, Cell Rep. 17 (2016) 1783–1794.
[10] J.D. Weaver, D.M. Headen, J. Aquart, C.T. Johnson, L.D. Shea, H. Shirwan, et al., Vasculogenic hydrogel enhances islet survival, engraftment, and function in leading extrahepatic sites, Sci. Adv. 3 (2017), e1700184.
[11] H. Wu, D. Wen, R.I. Mahato, Third-party mesenchymal stem cells improved human islet transplantation in a humanized diabetic mouse model, Mol. Ther. 21 (2013) 1778–1786.
[12] N. Marek-Trzonkowska, M. Mysliwec, J. Siebert, P. Trzonkowski, Clinical application of regulatory T cells intype 1 diabetes, Pediatr. Diabetes 14 (2013) 322–332.
[13] A.N. McMurchy, A. Bushell, M.K. Levings, K.J. Wood, Moving to tolerance: clinical application of T regulatory cells, Semin. Immunol. 23 (2011) 304–313.
[14] F. Issa, K.J. Wood, The potential role for regulatory T-cell therapy in vascularized composite allograft transplantation, Curr. Opin. Organ Transplant. 19 (2014) 558–565.
[15] N. Marek, A. Krzystyniak, I. Ergenc, O. Cochet, R. Misawa, L.J. Wang, et al., Coating human pancreatic islets with CD4(+)CD25(high)CD127(-) regulatory T cells as a novel approach for the local immunoprotection, Ann. Surg. 254 (2011) 512–518, discussion 518-519.
[16] K. Golab, S. Kizilel, T. Bal, M. Hara, M. Zielinski, R. Grose, et al., Improved coating of pancreatic islets with regulatory T cells to create local immunosuppression by using the biotin-polyethylene glycol-succinimidyl valeric acid ester molecule, Transplant. Proc. 46 (2014) 1967–1971.
[17] H.W. Lim, H.E. Broxmeyer, C.H. Kim, Regulation of trafficking receptor expression in human forkhead box P3+ regulatory T cells, J. Immunol. 177 (2006) 840–851.
[18] E.M. Shevach, CD4+ CD25+ suppressor T cells: more questions than answers, Nat. Rev. Immunol. 2 (2002) 389–400.
[19] K. Golab, S. Kizilel, T. Bal, M. Hara, M. Zielinski, X.J. Wang, et al., Biotin-peg-sva as a more effective linking molecule in comparison to biotin-PEG-NHS for coating of pancreatic islets with regulatory T cells (Tregs) to create local immunoprotection - optimization of the method, Transplantation 96 (2013). S63-S63.
[20] B. Brooks-Worrell, T. Tree, S.I. Mannering, I. Durinovic-Bello, E. James, P. Gottlieb, et al., Comparison of cryopreservation methods on T-cell responses to islet and control antigens from type 1 diabetic patients and controls, Diabetes Metab. Res. Rev. 27 (2011) 737–745.
[21] J.F. Jacobs, S. Nierkens, C.G. Figdor, I.J. de Vries, G.J. Adema, Regulatory T cells in melanoma: the final hurdle towards effective immunotherapy? Lancet Oncol. 13 (2012) e32–42.
[22] E. Elinav, R. Nowarski, C.A. Thaiss, B. Hu, C.C. Jin, R.A. Flavell, Inflammation-induced cancer: crosstalk between tumours, immune cells and microorganisms, Nat. Rev. Canc. 13 (2013) 759–771.
[23] A. Facciabene, G.T. Motz, G. Coukos, T-regulatory cells: key players in tumor immune escape and angiogenesis, Cancer Res. 72 (2012) 2162–2171.
[24] N. Fotino, C. Fotino, A. Pileggi, Re-engineering islet cell transplantation, Pharmacol. Res. 98 (2015) 76–85.
[25] M. McCall, A.M. Shapiro, Islet cell transplantation, Semin. Pediatr. Surg. 23 (2014) 83–90.
[26] W. Staels, S. De Groef, Y. Heremans, V. Coppens, N. Van Gassen, G. Leuckx, et al., Accessory cells for beta-cell transplantation, Diabetes Obes. Metab. 18 (2016) 115–124.
[27] A. Masamune, K. Kikuta, T. Watanabe, K. Satoh, M. Hirota, T. Shimosegawa, Hypoxia stimulates pancreatic stellate cells to induce fibrosis and angiogenesis in pancreatic cancer, Am. J. Physiol. Gastrointest. Liver Physiol. 295 (2008) G709–G717.
[28] Z. Yin, W. Wu, J.J. Fung, L. Lu, S. Qian, Cotransplanted hepatic stellate cells enhance vascularization of islet allografts, Microsurgery 27 (2007) 324–327.
[29] M. Erkan, C. Reiser-Erkan, C.W. Michalski, S. Deucker, D. Sauliunaite, S. Streit, et al., Cancer-stellate cell interactions perpetuate the hypoxia-fibrosis cycle in pancreatic ductal adenocarcinoma, Neoplasia 11 (2009) 497–508.
[30] G. Jiang, H.R. Yang, L. Wang, G.M. Wildey, J. Fung, S. Qian, et al., Hepatic stellate cells preferentially expand allogeneic CD4+ CD25+ FoxP3+ regulatory T cells in an IL-2-dependent manner, Transplantation 86 (2008) 1492–1502.
[31] F.A. Schildberg, A. Wojtalla, S.V. Siegmund, E. Endl, L. Diehl, Z. Abdullah, et al., Murine hepatic stellate cells veto CD8 T cell activation by a CD54-dependent mechanism, Hepatology 54 (2011) 262–272.
[32] H.R. Yang, H.S. Chou, X. Gu, L. Wang, K.E. Brown, J.J. Fung, et al., Mechanistic insights into immunomodulation by hepatic stellate cells in mice: a critical role of interferon-gamma signaling, Hepatology 50 (2009) 1981–1991.
[33] H.R. Yang, C.C. Hsieh, L. Wang, J.J. Fung, L. Lu, S. Qian, A critical role of TRAIL expressed on cotransplanted hepatic stellate cells in prevention of islet allograft rejection, Microsurgery 30 (2010) 332–337.
[34] R. Charles, H.S. Chou, L. Wang, J.J. Fung, L. Lu, S. Qian, Human hepatic stellate cells inhibit T-cell response through B7-H1 pathway, Transplantation 96 (2013) 17–24.

[35] D. Tang, J. Gao, S. Wang, Z. Yuan, N. Ye, Y. Chong, et al., Apoptosis and anergy of T cell induced by pancreatic stellate cells-derived galectin-1 in pancreatic cancer, Tumour. Biol. 36 (2015) 5617–5626.
[36] A. Ene-Obong, A.J. Clear, J. Watt, J. Wang, R. Fatah, J.C. Riches, et al., Activated pancreatic stellate cells sequester CD8+ T cells to reduce their infiltration of the juxtatumoral compartment of pancreatic ductal adenocarcinoma, Gastroenterology 145 (2013) 1121–1132.
[37] T.A. Mace, Z. Ameen, A. Collins, S. Wojcik, M. Mair, G.S. Young, et al., Pancreatic cancer-associated stellate cells promote differentiation of myeloid-derived suppressor cells in a STAT3-dependent manner, Cancer Res. 73 (2013) 3007–3018.
[38] K. Kikuta, A. Masamune, S. Hamada, T. Takikawa, E. Nakano, T. Shimosegawa, Pancreatic stellate cells reduce insulin expression and induce apoptosis in pancreatic beta-cells, Biochem. Biophys. Res. Commun. 433 (2013) 292–297.
[39] G. Zang, M. Sandberg, P.O. Carlsson, N. Welsh, L. Jansson, A. Barbu, Activated pancreatic stellate cells can impair pancreatic islet function in mice, Ups. J. Med. Sci. 120 (2015) 169–180.
[40] N. Kojima, In vitro reconstitution of pancreatic islets, Organogenesis 10 (2014) 225–230.
[41] T. Bhaiji, Z.L. Zhi, J.C. Pickup, Improving cellular function and immune protection via layer-by-layer nanocoating of pancreatic islet β-cell spheroids cocultured with mesenchymal stem cells, J. Biomed. Mater. Res. A 100 (2012) 1628–1636.
[42] E. Vagesjo, G. Christoffersson, T.B. Walden, P.O. Carlsson, M. Essand, O. Korsgren, et al., Immunological shielding by induced recruitment of regulatory T-lymphocytes delays rejection of islets transplanted in muscle, Cell Transplant. 24 (2015) 263–276.
[43] N.G. Kooreman, P.E. de Almeida, J.P. Stack, R.V. Nelakanti, S. Diecke, N.Y. Shao, et al., Alloimmune responses of humanized mice to human pluripotent stem cell therapeutics, Cell Rep. 20 (2017) 1978–1990.
[44] C.F. Lee, Y.C. Lo, C.H. Cheng, G.J. Furtmuller, B. Oh, V. Andrade-Oliveira, et al., Preventing allograft rejection by targeting immune metabolism, Cell Rep. 13 (2015) 760–770.
[45] E.A. Ryan, J.R. Lakey, R.V. Rajotte, G.S. Korbutt, T. Kin, S. Imes, et al., Clinical outcomes and insulin secretion after islet transplantation with the Edmonton protocol, Diabetes 50 (2001) 710–719.
[46] J.L. Contreras, C. Eckstein, C.A. Smyth, M.T. Sellers, M. Vilatoba, G. Bilbao, et al., Brain death significantly reduces isolated pancreatic islet yields and functionality in vitro and in vivo after transplantation in rats, Diabetes 52 (2003) 2935–2942.
[47] H.S. Chou, C.C. Hsieh, H.R. Yang, L. Wang, Y. Arakawa, K. Brown, et al., Hepatic stellate cells regulate immune response by way of induction of myeloid suppressor cells in mice, Hepatology 53 (2011) 1007–1019.
[48] C.H. Chen, L.M. Kuo, Y. Chang, W. Wu, C. Goldbach, M.A. Ross, et al., In vivo immune modulatory activity of hepatic stellate cells in mice, Hepatology 44 (2006) 1171–1181.
[49] G. Cavallari, R.A. Zuellig, R. Lehmann, M. Weber, W. Moritz, Rat pancreatic islet size standardization by the "hanging drop" technique, Transplant. Proc. 39 (2007) 2018–2020.
[50] R. Lehmann, R.A. Zuellig, P. Kugelmeier, P.B. Baenninger, W. Moritz, A. Perren, et al., Superiority of small islets in human islet transplantation, Diabetes 56 (2007) 594–603.
[51] J. Montane, M. Obach, S. Alvarez, L. Bischoff, D.L. Dai, G. Soukhatcheva, et al., CCL22 prevents rejection of mouse islet allografts and induces donor-specific tolerance, Cell Transplant. 24 (2015) 2143–2154.
[52] J. Montane, L. Bischoff, G. Soukhatcheva, D.L. Dai, G. Hardenberg, M.K. Levings, et al., Prevention of murine autoimmune diabetes by CCL22-mediated Treg recruitment to the pancreatic islets, J. Clin. Investig. 121 (2011) 3024–3028.
[53] L. Bischoff, S. Alvarez, D.L. Dai, G. Soukhatcheva, P.C. Orban, C.B. Verchere, Cellular mechanisms of CCL22-mediated attenuation of autoimmune diabetes, J. Immunol. 194 (2015) 3054–3064.
[54] S. Jhunjhunwala, G. Raimondi, A.J. Glowacki, S.J. Hall, D. Maskarinec, S.H. Thorne, et al., Bioinspired controlled release of CCL22 recruits regulatory T cells in vivo, Adv. Mater. 24 (2012) 4735–4738.
[55] Y.Y. Wan, R.A. Flavell, Regulatory T-cell functions are subverted and converted owing to attenuated Foxp3 expression, Nature 445 (2007) 766.
[56] Z. Li, D. Li, A. Tsun, B. Li, FOXP3+ regulatory T cells and their functional regulation, Cell. Mol. Immunol. 12 (2015) 558.
[57] X. Zhou, S.L. Bailey-Bucktrout, L.T. Jeker, C. Penaranda, M. Martínez-Llordella, M. Ashby, et al., Instability of the transcription factor Foxp3 leads to the generation of pathogenic memory T cells in vivo, Nat. Immunol. 10 (2009) 1000.
[58] C.M. Hull, M. Peakman, T.I. Tree, Regulatory T cell dysfunction in type 1 diabetes: what's broken and how can we fix it? Diabetologia 60 (2017) 1839–1850.
[59] M. Erkan, N. Weis, Z. Pan, C. Schwager, T. Samkharadze, X. Jiang, et al., Organ-, inflammation- and cancer specific transcriptional fingerprints of pancreatic and hepatic stellate cells, Mol. Cancer 9 (2010) 88.
[60] M. Erkan, G. Adler, M.V. Apte, M.G. Bachem, M. Buchholz, S. Detlefsen, et al., StellaTUM: current consensus and discussion on pancreatic stellate cell research, Gut 61 (2012) 172–178.
[61] T.T. Onder, N. Kara, A. Cherry, A.U. Sinha, N. Zhu, K.M. Bernt, et al., Chromatin-modifying enzymes as modulators of reprogramming, Nature 483 (2012) 598–602.